Geomechanics and Engineering, *Vol. 26, No. 4 (2021) 357-367*
https://doi.org/10.12989/gae.2021.26.4.357

Influence of a preset fissure on clay behavior under uniaxial compression

Wei Wang*, Binghua Zhao[a], Aiyu Hu[b] and Jibin Shang[b]

School of Civil Engineering, Nanjing Institute of Technology, Nanjing 211167, China

(Received July 10, 2020, Revised June 13, 2021, Accepted August 5, 2021)

Abstract. Under compression, the flaws in soils will not only weaken the mechanical properties of soils, but also affect the strain localization of soils. In order to study the influence of flaws on the behavior of soils under compression, the uniaxial compression tests of clays with different inclination and position fissures were carried out, and the two-dimensional numerical analysis was also discussed based on the damage plasticity model. Analyzing the results of the uniaxial compression test and simulation of the intact and fissured clays, the following conclusions can be drawn: (1) The 60-degree fissure located on the upper position of the right edge of the clay has the greatest influence on the failure form and damage energy of clays, which can reduce the compression strength by 30% compared with that of the intact clay. (2) The numerical method based on the damage plasticity model can basically simulate the compression behavior of clays containing a pre-existing fissure and reproduce the failure characteristics of clays. (3) The preset fissure has obvious influence on the evolution of maximum principal stress in the area with serious damage, but less on the shear stress. And in the area with slight damage, the effect on the maximum principal stress and shear stress is very weak.

Keywords: failure; fissured clay; local damage; numerical simulation; uniaxial compression

1. Introduction

Flaws (cracks or holes) in soils caused by external factors are often found in the geotechnical engineering. The existence of flaws leads to the geometric discontinuity of soils, which means that there is an initial local damage in soils. This not only weakens the mechanical properties of soils, but also changes the failure form of soils, which will bring great hidden trouble to the safety of geotechnical engineering. If the development and evolution of these flaws under loads and its influence mechanism on failure form of defective soils are clarified, it will be of great practical significance for soil crack monitoring and prevention, slope stability evaluation and underground engineering construction.

Under compression, the soil has the characteristics of gradual failure, and most of them will also appear the strain localization (shear zone). The compression characteristics and deformation evolution mechanism of soils have always been a hot topic in the field of geotechnical mechanics. In particular, the research on the formation and development of shear zone has made a series of rich achievements, but most of them are mainly aimed at the intact soil samples. For example, using the compression test of intact sand samples, Wanatowski and Chu (2006) found that dense sand or medium dense sand is easy to form shear zone, but loose sand is not. In fact, the traditional compression test is to treat the soil sample as a single element, and the whole stress-strain relationship and deformation failure form can be obtained under different stress paths. However, the evolution of local deformation for soil samples cannot be obtained, and the gradual failure process of soils cannot be quantitatively described. With the introduction of advanced testing instruments and testing methods, visual testing methods have become the mainstream in the field of geotechnical researches. For instance, Watanabe et al (2012) used X-ray CT to measure the distribution of the localized displacement in sand under triaxial compression. Vangla and Latha (2015) investigated the effect of size of the particles on the shear and interfacial shear strength of sands through direct shear and interface direct shear tests complemented with image analyses. Desrues *et al.* (1996) studied the strain localization in trial tests on sand using the computed tomography and pointed out that a limit void ratio is reached in the shear zones by the comparison of the local void ratio evolution in the shear zones with the global void ratio. The above visual experimental studies still consider soil samples as an intact structure, and such limited analysis in microscopic views is far from adequate to obtain a comprehensive understanding of the shear band in soils.

Similar research ideas are also reflected in theoretical analysis and numerical simulation. For describing the strain softening properties of soils, some scholars have developed related theories, such as bifurcation theory, homogenization approach, nonlocal strain theory, gradient plasticity theory, etc. Based on these theories, the local strain failure of soils has been analyzed numerically. For instance, Borja (2004) discussed the formation of deformation bands in geomaterials based on the bifurcation theory. Mühlhaus and Alfantis (1991) demonstrated the gradient plasticity model to estimate the width and spacing of shear bands. For

*Corresponding author, Associate Professor, Ph.D.
E-mail: ww1177114@163.com
[a]Associate Professor
[b]Lecturer

ISSN: 2005-307X (Print), 2092-6219 (Online)

numerical simulation, many researchers have studied the influence mechanism of soil sample boundary conditions (Ebrahimian *et al.* 2018), particles (pores) state (Bayesteh and Ghasempour 2019), physical properties (Kozicki and Tejchman 2018; Jiang et al 2018), stress paths (Liang *et al.* 2019; Huang *et al.* 2015) and so forth on local failure and shear zone formation by the discrete element method or finite element method.

The above excellent researches are mainly for the compressive mechanical properties of granular media such as intact sand, less for the compression failure of geometric discontinuous clays or clays containing geometric flaws. Although, a few scholars characterized the discontinuity of soil samples by setting a weak element (or zone) in the numerical model (Schneider-Muntau *et al.* 2017), the discontinuity belongs to the material discontinuity of soils, not the geometric discontinuity of soils. While, the study of compression failure for geometric discontinuous rocks and rock-like materials is more common. These geometric discontinuities mainly refer to multiple forms of defects in rocks or rock-like materials, such as a defect, two fissures or holes, multiple fissures, one hole and two fissures coexisting. Many scholars have mainly studied the propagation evolution of the preset fissures and its influence mechanism on the failure forms of rocks or rock-like materials. For example, Castelli *et al.* (2009) investigated the progressive shear failure in rocks as the result of shear propagation of a pre-existing natural defect. Huang *et al.* (2019) researched the crack propagation process, rupture angle, and strength of a rocklike material containing a single large-opening crack under uniaxial compression. Besides that, rocks or rock-like materials with two fissures or holes were also analyzed. Wang *et al.* (2012) found that the side ratio and distance between two cracks exerted an obvious influence on the interaction between two coplanar or parallel rectangular cracks. Huang *et al.* (2016) carried out uniaxial compression tests for rock-like specimens with two unparallel fissures to research the mechanical properties and crack coalescence process. Dong *et al.* (2019) studied the mechanical behavior and cracking pattern of natural marble with double S-shaped fissures under compression loading. Xu *et al.* (2017) gave an insight into the understanding of damage evolution and crack propagation in rocks with dual elliptic flaws. Moreover, for multiple fissures, both disordered and ordered fissures were studied. Wang *et al.* (2020) pointed out that the strength with more new cracks is not necessarily less than that of rock specimens with fewer new cracks and the failure of rock is caused by the formation of macro-fracture surface. Wang *et al.* (2017) analyzed the influence of both the number of pre-cracks and pre-cracks angles on crack growth. Also, rock with one hole and two fissures was discussed. Yang *et al.* (2014) investigated the effect of crack coalescence process on the strength and deformation behavior of brittle sandstone specimens containing combined flaws (a hole and two coplanar fissures passed through the center of the hole) under uniaxial compression. As we know, the physical and mechanical properties of rocks or rock-like materials are different from that of soils, so the research results for rock or rock-like materials cannot be directly used for soils. It is necessary to carry out further research on soils considering the existence of flaws.

Based on the above analysis, this paper studies the influence mechanism of fissures on failure form and local deformation of clays under uniaxial compression by means of test and numerical method. Firstly, the geometric discontinuity of clays is realized by presetting fissures (just like the geometric discontinuity of rocks, furthermore, the geometric discontinuity of clays is easier to realize), and then the uniaxial compression test is carried out to observe the influence of fissures on failure form of the fissured clays. Finally, the influence mechanism of fissures on local deformation of the fissured clays is analyzed by numerical method, which provides a deep understanding of the compression behavior of geometric discontinuous clays.

2. Materials and uniaxial compression test

2.1 Clay sample for test

The purpose of this paper is to explore the correlation between the existing fissures and failure form of clays under uniaxial compression, so the one-dimensional compression state of normal consolidated clay is analyzed. In order to observe and photograph the evolution of cracks under uniaxial compression and the influence process on local deformation of clays through the digital camera, the observed surface of clay needs to be a plane. Therefore, according to the principle of axial symmetry, the conventional cylindrical clay sample is divided into two parts along the axis of symmetry. Then, the geometric discontinuous clay sample is formed by presetting fissures on the semi-cylindrical clay sample as the test object, and the axisymmetric surface is taken as the observation plane. Here, the selected one is a semi-cylindrical clay sample with a diameter of 39.1 mm and a height of 80 mm (The compression test and simulation of the cylindrical clay with preset fissures and the influence of the third dimension will be studied in the next step). Fig. 1 shows the photo of the one-dimensional compression test device (taking T_{22} as an example). Table 1 lists the physical properties of the clay sample.

The clay sample were prepared using the remolded clay. First, the natural clay was dried by the wind, and then crushed. After passing through the 2mm sieve, the moisture content of the clay was measured. Then, the clay material and water required for preparing the clay samples were evenly mixed and cured for 24 hours. Next, the cured clay was compacted to the required cylindrical clay sample. Finally, using the 0.2 mm thin blade, the cylindrical clay sample was divided into two semi-cylindrical specimens and the preset fissures were also made on the semi-cylindrical clay sample, respectively. The shape of the edges of the fissure with 0.5 mm width and 16mm length is basically V-shape.

Before loading in the compression test, the upper and lower surfaces of the prepared clay sample were applied

Table 1 Physical properties of the clay sample

Relative density	Water content (%)	Liquid limit (%)	Plastic limit (%)	Dry density (g/cm^3)	Plastic index
2.70	18.01	33.65	18.98	1.90	14.67

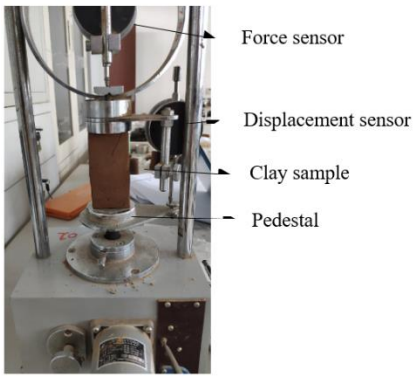

Fig. 1 One-dimensional compression test device (taking T_{22} as an example)

Table 2 Clay samples with a pre-existing fissure

Fissure location		Middle of the upper edge	Right side of the upper edge (About 5 mm between upper tip and right edge)	Upper position of the right edge (About 5 mm between upper tip and right edge, also and upper edge)
Fissure angle*	90°	T_{11}	T_{21}	T_{31}
	60°	T_{12}	T_{22}	T_{32}
	30°	T_{13}	T_{23}	T_{33}

*Fissure angle: means the angle between the pre-existing fissure and the horizontal line

Vaseline. Then, the loading was applied on the upper surface of the sample located on the pedestal of the instrument at a rate of 0.2mm per minute until the clay sample finally destroyed or reached the strain 0.2. Three test samples were made for each fissure type. The detailed two-dimensional fissure types are shown in Table 2. The test results show that the maximum strain of compression test is 12.5%, that is, the maximum compression displacement is 10mm.

2.2 Test results

Only by comparing with the compression failure forms of the intact clay can the influence of existing fissures on the failure form and local deformation of clays be better studied. Therefore, the uniaxial compression test of the intact clay and the fissured clays were all carried out. Here, for consistency, semi-cylindrical intact clay sample was also chosen. Table 3 shows the final failure forms of the intact clay and nine fissured clays.

From the final failure forms shown in Table 3, we learn that the bulge of the upper half in each clay sample occurred under uniaxial compression. However, the position and inclination of the pre-existing fissure have certain influence on the failure form of the fissured clays, and the final failure form is different from that of the intact clay. Specifically, (1) When the fissure is located in the middle of the upper edge of the clay sample, the 90-degree fissure width is increased than before loading, but there is no obvious propagation. While, the 60-degree and 30-degree fissures are closed under the loadings. In addition, the three kinds of preset fissures have no influence on the appearance of new cracks in clay samples. (2) When the fissure is located at the right side of the upper edge, the 60-degree fissure causes the clay sample to appear oblique crack, and the oblique crack intersects with the 60-degree fissure tip. But the 90-degree and 30-degree fissures have no obvious influence on the appearance of new cracks in clay samples. (3) When the fissure is located on the right edge, the clay sample with 90-degree fissure occurs local bending failure at the fissure, while the 30-degree fissure is closed under the compression. Specially, the 60-degree fissure causes the upper clay to slide along the preset fissure surface, forming an inclined crack through the clay, and there is obvious crushing at the tip of the preset fissure, which is more serious than that of other clay samples with the preset fissure. In brief, for the fissure position, the preset fissure

Table 3 Test results for clay samples

Type of clay sample	Test result	Type of clay sample	Test result
Intact clay		T_{22}	
T_{11}		T_{23}	
T_{12}		T_{31}	
T_{13}		T_{32}	
T_{21}		T_{33}	

on the right edge has a great influence on the clay damage, and for the fissure angle, the influence caused by the 60-degree fissure is more serious than that of the other angles fissure.

Simultaneously, from the nominal axial stress-axial strain curve of clay samples shown in Fig. 2, it can be not only found that the uniaxial compression behavior of the semi-cylindrical clay sample is manifested as elastic-plastic deformation, regardless of the presence of the fissure or not, but also quantitatively concluded that the compressive strength of clay containing a fissure is lower than that of the intact clay. The compressive strength of the clay sample type T_{32} is the lowest, about 70% of the compressive strength of the intact clay, and its corresponding strain is the smallest, about 80% of the axial strain of the intact clay. Obviously, the 60-degree fissure located on the right edge has the greatest influence on the compression failure of the fissured clay, which not only reduces the compressive strength of the clay but also weakens its plasticity.

3. Numerical simulation

The stress-strain curve mentioned above is the result of treating the clay sample as a unit, but it cannot reflect the evolution characteristics of local stress-strain in the clay. Obviously, the experimental results show that local damage occurs in both intact and fissured clay samples during compression, which can be interpreted as strain localized instability failure based on the bifurcation theory. For a more in-depth study of the influence mechanism of preset fissure on failure form and local damage of clays, ABAQUS software was used to carry out numerical analysis based on the damage plasticity model.

3.1 Numerical model

Based on the ABAQUS platform, the numerical model of the clay sample is a two-dimensional model, and the size

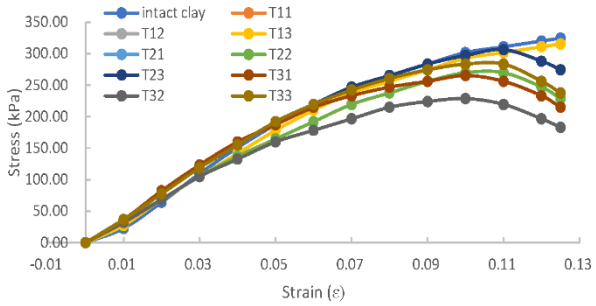

Fig. 2 Stress-strain curves of clay samples

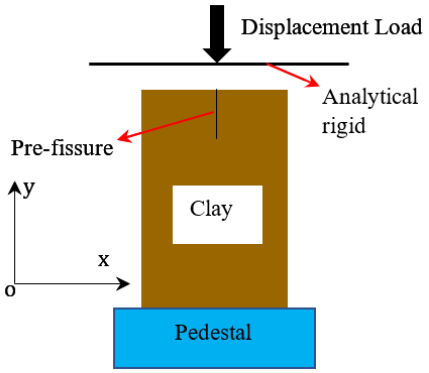

Fig. 3 Schematic diagram of clay model under loading

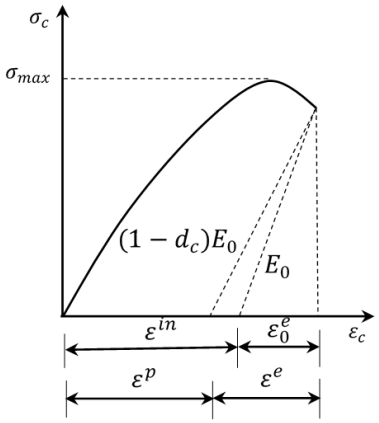

Fig. 4 Stress-strain curve under uniaxial compression

and fissure form are consistent with those listed in Table 1, which is a total of nine models. Displacement loading is selected to apply on the model, and the maximum displacement of 10 mm is the same as the final compression value of the test result. In order to be as consistent as possible with the test boundary conditions, the displacement loads are applied on the numerical model by the analytical rigid. The schematic diagram of clay sample under loading (taking the model T_{11} as an example) is depicted in Fig. 3. Subsequently, numerical compression tests for clay models were carried out using plane stress element type.

3.2 Damage plasticity model

Plastic deformation and stiffness degradation occur in clays under compression, as shown in Fig. 4 (in figure, ε^{in} is the inelastic strain, ε_0^e is the elastic strain without considering the compression damage, ε^e is the elastic strain taking the compression damage into account, ε^p is the plastic strain). So, the compression damage factor (d_c) is introduced to reflect the decline of stiffness and its expression is shown in the Eq. (1).

Table 4 Plastic parameters used for clay models

Plasticity parameters	values
Dilation angle (ψ)*	0.1
Eccentricity (ϵ)	0.1
Ultimate strength ratio (f_{b0}/f_{c0})	1.16
Invariable stress ratio (K)	0.667
Viscosity parameter (μ)	0.0003-0.0005

*Eccentricity (ϵ): is flow potential offset and taken to 0.1; Ultimate strength ratio (f_{b0}/f_{c0}): is the ratio of biaxial ultimate compressive strength and uniaxial compressive ultimate strength obtained by biaxial and uniaxial compression test; Invariable stress ratio (K): is the ratio of the second stress invariant on the tensile meridian to the compressed meridian and taken to 0.667; Viscosity parameter (μ): defines the viscosity rule of clays, which is helpful to the convergence of numerical calculation

$$d_c = \frac{(1-\beta_c)\varepsilon^{in}E_0}{\sigma_c + (1-\beta_c)\varepsilon^{in}E_0} \tag{1}$$

where, $\beta_c = \frac{\varepsilon^p}{\varepsilon^{in}}$, E_0 is the elasticity modulus.

By modifying the initial elastic stiffness, the stress-strain relation for the clay is as follows:

$\sigma = (1-d_c)D_0^e : (\varepsilon - \varepsilon^p)$. Where, D_0^e is the initial elastic stiffness without considering the damage, ε is the total strain.

The model adopted the non-associated flow criterion, shown in the Eq. (2).

$$\mathrm{d}\varepsilon^p = \mathrm{d}\lambda \frac{\partial g}{\partial \sigma} \tag{2}$$

where, $\mathrm{d}\lambda$ is the proportional constant, g is the plastic potential function, which is taken as Drucker-Prager hyperbolic equation:

$$g = \sqrt{(\eta\sigma_t \tan\psi)^2 + \bar{q}^2} - \bar{p}\tan\psi = 0$$

Where, ψ is the dilation angle, η is the eccentricity of plastic potential function for clays, σ_t is the uniaxial tensile strength of clays, $\bar{p}$ is the effective hydrostatic pressure, and $\bar{q}$ is the Mises stress.

Based on the compression tests and analysis aforementioned, the damage plasticity model was adopted in the numerical method. According to the definition of the material property, the inelastic strain and the corresponding yield stress need to be calculated and input from the test data. Then, using the Eqs. (3) and (4), the inelastic strain of clay can be obtained.

$$\varepsilon = \varepsilon_0^e + \varepsilon^{in} \tag{3}$$

$$\varepsilon_0^e = \frac{\sigma_c}{\mathrm{E}_0} \tag{4}$$

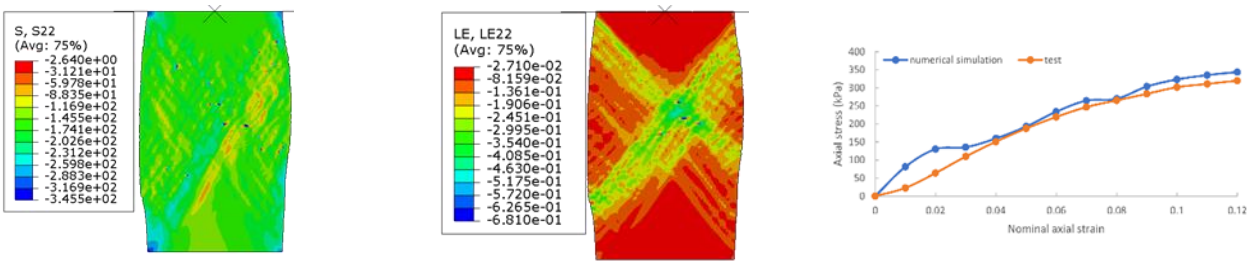

(a) Axial stress contour (b) Axial strain contour (c) Stress-strain curve

Fig. 5 Simulation results for the intact clay under compression

Table 5 Stress-strain curve of 9 clay models with a fissure

T_{11} 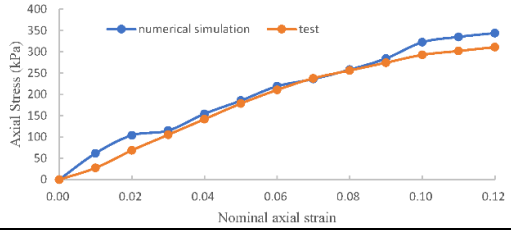	T_{23} 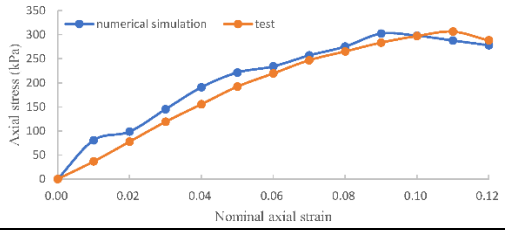
T_{12} 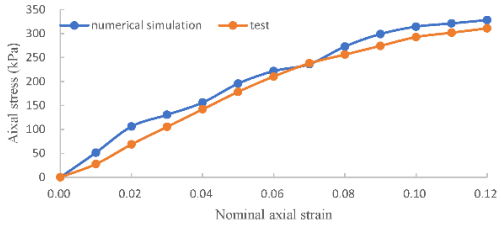	T_{31} 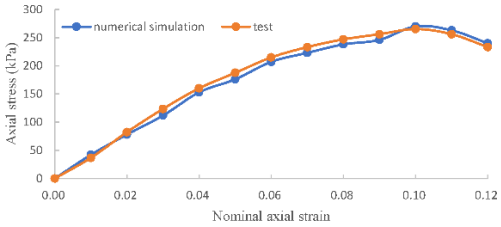
T_{13} 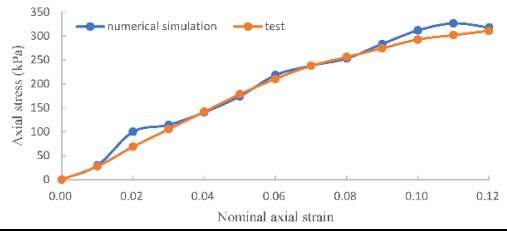	T_{32} 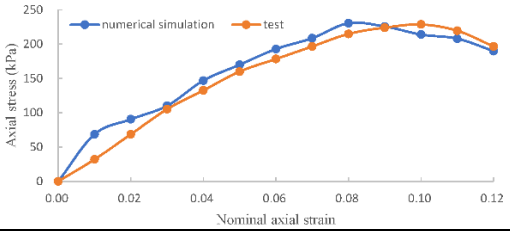
T_{21} 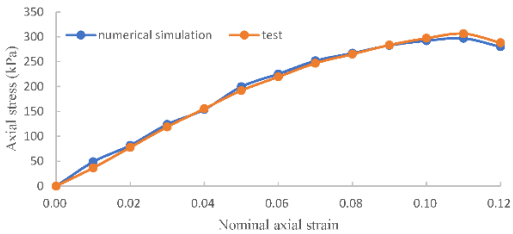	T_{33} 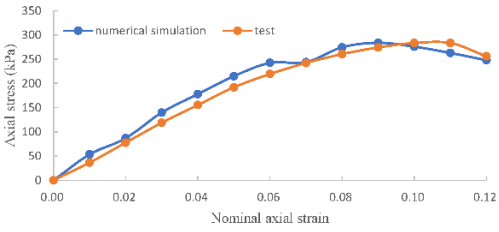
T_{22} 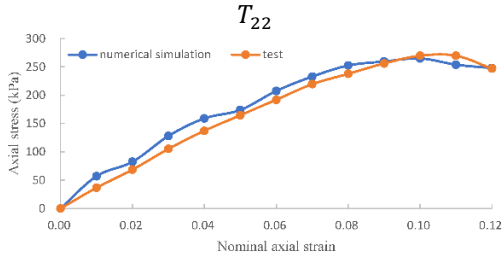	

So,

$$\varepsilon^{in} = \varepsilon - \frac{\sigma_c}{\mathrm{E}_0}$$

After the inelastic strain of each clay sample under the compression test were all calculated, the corresponding stress were also found from the stress-strain curve. As we

Table 6 The simulation results of compression damage for clays

Type of clay sample	Contour of compression damage	Type of clay sample	Contour of compression damage
Intact clay	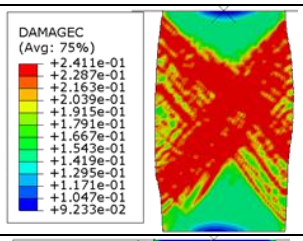	T_{22}	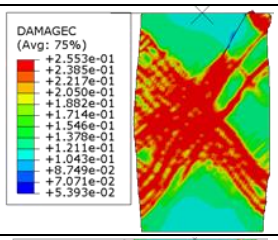
T_{11}	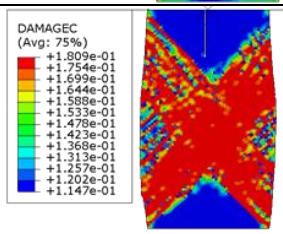	T_{23}	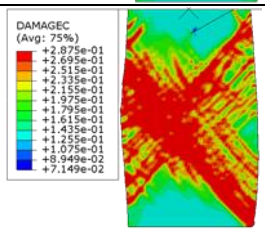
T_{12}	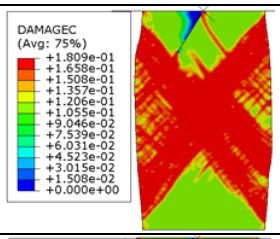	T_{31}	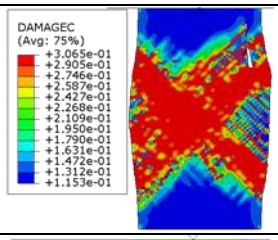
T_{13}	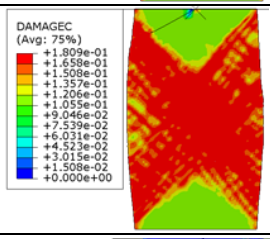	T_{32}	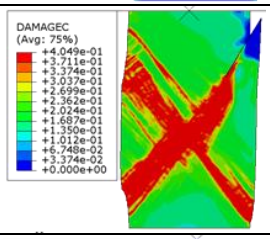
T_{21}	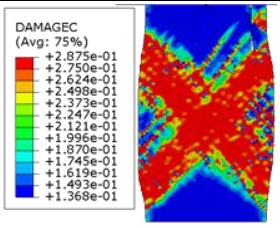	T_{33}	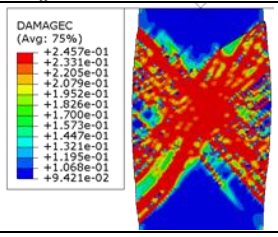

know, the dilatancy is ignored for the normal consolidated clay. Then, the dilation angle (ψ) is set to 0.1, here.

After trial calculations and adjustments, the other plastic parameters are taken as shown in Table 4.

3.3 Definition of contact surfaces under compression

There are two pairs of contact surfaces in the compression process of the fissured clay. First, the analytical rigid above the clay model as the loading device (similar to the loading plate in the test) is in contact with the upper surface of the clay sample. The second is the preset fissure in the clay model, and the fissure surface will also be in self-contact when the clay model is compressed. Therefore, the interaction mechanical model of contact surfaces needs to be defined. The contact between the loading plate and the clay sample belongs to the contact between the rigid body and the deformed body, which is divided into the master-slave surface (the rigid body is the master surface, and the deformed body is the slave surface). The mechanical properties of the contact are as follows: the normal behavior of the contact surface is hard contact, and the tangential behavior conforms to the Coulomb law. In view of the application of Vaseline (reducing friction) on the loading plate surface before loading, the friction coefficient is 0.2. For the contact of fissure surface for the clay sample during compression, it belongs to the clay self-contact. The mechanical characteristics of the contact are as follows: the normal behavior of the contact surface is still hard contact, and the tangent behavior can be taken as the tangent value of the internal friction angle. That is $\tan\varphi = \tan 29°$=0.55 (φ is the internal friction angle of remolded clay. $\varphi = 29°$).

3.4 Simulation results

3.4.1 Axial stress-strain curve

Limited to space, the axial stress contour and axial strain

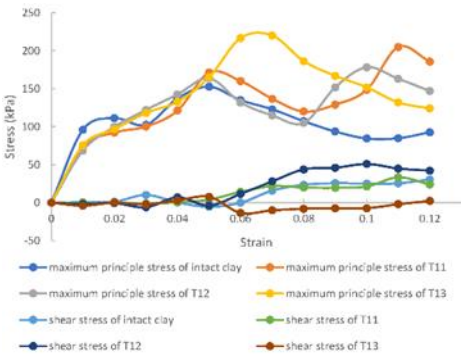

(a) Intact clay and clay with a fissure located in the middle of the upper edge

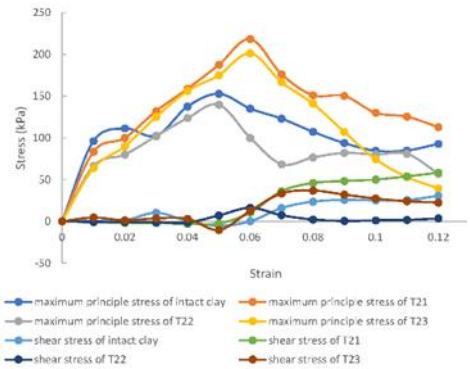

(b) Intact clay and clay with a fissure located at the right side of the upper edge

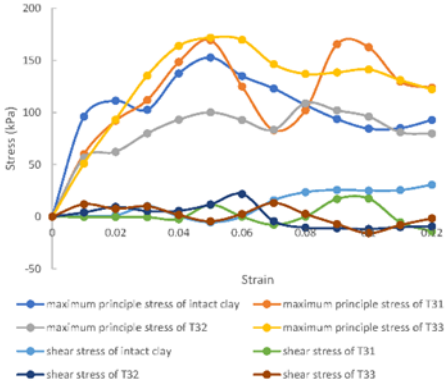

(c) Intact clay and clay with a fissure located on the right edge

Fig. 6 Stress-strain curve in severely damaged areas

contour of the intact clay are taken as an example, shown in Figs. 5(a) and 5(b), respectively. Then, analyzing the contours, we can learn that the clay is not uniformly deformed under uniaxial compression, nor does each point reach the maximum stress at the same time. In fact, the maximum stresses are mostly concentrated at the four corners of the clay sample, and the shape of larger strains is cross-banded, such as X-pattern, which is called strain localization. The blue line in Fig. 5(c) represents the axial stress-strain curve at the lower left corner of the clay sample, and its evolution law is basically similar to the compression test results of the clay (indicated by the orange line). In other words, the coincidence degree is high. In detail, under the same nominal strain (0.12), the maximum compressive stress in the numerical results is 344.03 kPa, which is close to the maximum compressive stress in the test, 320.1 kPa. The error between the maximum stresses is 7.5%. It shows that the numerical method can reflect the uniaxial compression behavior of clays.

Table 5 shows the axial stress-strain curves of 9 clay models with preset fissure through compression simulations and tests.

It can be seen from Table 5 that similar to the axial compression results of the intact clay, the stress-strain curves of 9 clay models with a fissure obtained from the numerical compression tests are basically the same with the corresponding test results. Therefore, using the damage plasticity model, the compression simulation for clays with a fissure can be realized.

3.4.2 Influence mechanism of fissures

From the damage contour of clays shown in Table 6, it can be seen that the more serious damage areas in the clay exhibit an X-pattern, and the location and width of the damage areas are different. Compared with the test results (shown in Table 3), it is found that the location of obvious cracks in the test clay samples is basically located in the damage serious area of the clay models (indicated in red). In addition, where there is no damage in the test clay samples, there is no obvious damage at the same position of the numerical models (As for the part of the test clay sample that the damage is not obvious is also located in the serious damage area of the numerical model, which may be related to the difference between the three-dimensional clay sample and the two-dimensional numerical model, and may also be related to the damage plasticity model adopted. It will be studied in future). But overall, this numerical method is feasible to simulate the compression damage of clays, although there is still a gap in the results.

Damage areas of X-pattern in all clay models are not exactly the same, which is shown in Table 6. It indicates that the existence of fissures has certain influence on the local damage and failure form of clays. (1) When the fissure is located in the middle of the upper edge of the clay sample, the serious damage area is similar to the intact clay, and all of them are divergent. (2) When the fissure is located at the right side of the upper edge or the upper side of the right edge of clays, the serious damage area is smaller than that of the intact clay. In particular, for clays containing

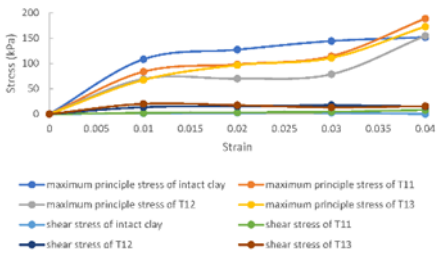

(a) Intact clay and clay with a fissure located in the middle of the upper edge

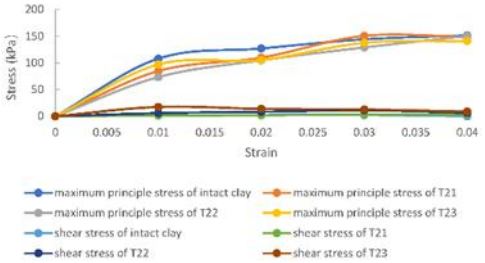

(b) Intact clay and clay with a fissure located at the right side of the upper edge

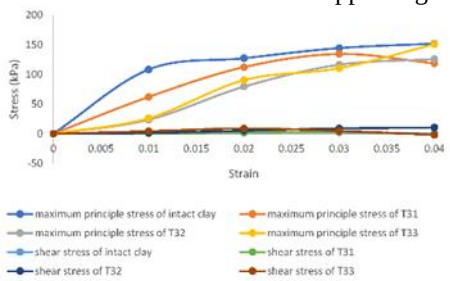

(c) Intact clay and clay with a fissure located on the right edge

Fig. 7 Stress-strain curve in slightly damaged areas

the 60-degree fissure, partial damage in the cross-damage zone is formed from the preset fissure tip and develops along the fissure direction, like that of the clay types T_{22} and T_{32}.

In order to explore the influence mechanism of fissures, the evolution characteristics of the maximum principal stress and shear stress with nominal strain in the slightly and severely damaged areas are obtained from the numerical results, shown in Fig. 6.

Except T_{32}, before the nominal strain reaches 0.05, the maximum principal stresses in the severely damaged areas of the fissured clays and the intact clay are almost the same, which indicates that the existence of fissures has no effect on the compression behavior of clay during the loading period. When the nominal strain is more than 0.05, the maximum principal stresses in the seriously damaged areas of each clay sample have obviously different evolution characteristics.

(1) No bimodal phenomenon appeared in the maximum principal stress-strain curves of the 30-degree fissured clays. Meanwhile, the strain corresponding to the maximum stress value is larger than that of the intact clay, at which time the strain is 0.06. This may be related to the time required for the fissure closure (both test and simulation results show that the 30-degree fissure is closed under compression), and once the fissure is closed, the fissured clay is like a whole to withstand loads, similar to the intact clay sample. This increases the strain and delays the arrival time of the maximum strain.

(2) For the 90-degree fissure, due to compression closure, the maximum principal stress-strain curve of the clay with the 90-degree fissure located at the right side of the upper edge also does not appear bimodal phenomenon, while in other positions, there are obvious bimodal characteristics. The possible reason is that the fissured clay forms a structure containing the pore, when the fissure is located in the middle position of the upper edge or on the right edge of the clay sample. With the increase of the strain, the fissure width is increasing, and the first peak point of the maximum principal stress and the strain softening appear when the pore structure is destroyed. Moreover, since the right fissure width is larger than that of the middle position fissure, the damage of the clay type T_{31} is also serious, which leads to the peak value of the maximum principal stress in the area with serious damage of the clay containing the right fissure lower than that of the one with the middle fissure. As the nominal strain continues to increase, the further hardening of the clay is dominant after the failure of the pore structure, resulting in the maximum principal stress-strain curve in the seriously damaged area starts to rise again. Soon, a second peak point of the maximum principal stress appears, indicating that the soil damage is further aggravated. This is different from the evolution law of the maximum principal stress in the serious damage area of the intact clay.

(3) According to the 60-degree fissure, the maximum principal stress in the seriously damaged area of clays is smaller than that of clays with other fissures. Moreover, it can be seen that the closer the 60-degree fissure is to the edge of the clay, the smaller the maximum principal stress in the area with serious damage.

For T_{32}, when the nominal strain exceeds 0.01, the damage is more obvious, and the clay slips along the inclined direction of the fissure, resulting in the maximum principal stress in the serious damage area is always lower than that of other clay samples. It is further proved that the preset fissure has the greatest influence on the failure form of the clay type T_{32}. In conclusion, the existence of fissures has an effect on the failure form and damage area of clays, especially the fissures are located on the right edge of clays.

From the shear stress-strain curves shown in Fig. 6, we

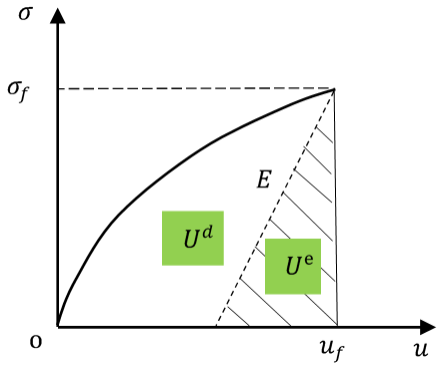

Fig. 8 Diagram of relationship between damage energy and elastic energy (E is elasticity modulus, σ_f is peak stress. And u_f is peak displacement)

Table 7 Damage energy and maximum axial stress of clays

Clay type	intact	T_{11}	T_{12}	T_{13}	T_{21}	T_{22}	T_{23}	T_{31}	T_{32}	T_{33}
Damage energy (kN/m)	1.6	1.55	1.55	1.55	1.29	1.03	1.27	1.13	0.96	1.09
Maximum axial stress (kPa)	152.7	205.0	178.2	220.0	218.2	139.6	201.2	169.3	108.9	171.8

learn that when the nominal strain is not more than 0.05, the evolution law of shear stress is basically the same and the stress value is about zero. When the nominal strain exceeds 0.05, although the evolution trend of shear stress in the serious damage area of clay samples is different, there is no obvious rule to follow. However, the values of shear stresses are small and the maximum values are generally less than 50 kPa. It can be seen that the influence of preset fissures on the shear stress in the serious damage area of clays under uniaxial compression is limited.

From the maximum principal stress-strain curves shown in Fig. 7, it is obtained that the nominal strain in the slightly damaged areas of clay samples is smaller, about 1/3 of the nominal axial strain. The maximum principal stress of clay samples increases with the increase of the strain, and the corresponding maximum principal stress of the fissured clays is basically lower than that of the intact clay. That is to say, the preset fissure has a weakening effect on the maximum principal stress in the slightly damaged areas. Especially, the influence degree of the fissure located on the right edge is more obvious, and the influence degree of the 60-degree fissure is slightly more obvious than other angle fissures.

The shear stress in the slightly damaged areas of clay samples is almost equal to zero, and the preset fissure has no obvious effect on the shear stress, which is similar to the evolution of the intact clay.

3.4.3 Damage energy

Based on the stress-strain curves obtained from the compression tests for clay samples, the damage energy called U^d is defined by the formula (5).

$$U^d = U - U^{\mathrm{e}} \tag{5}$$

where, U is the total energy, that is the area surrounded by the stress-displacement curve and the abscissa, $U = \int \sigma du$. And U^{e} is the elastic energy which is the shadow area shown in Fig. 8.

According to the stress-strain curves shown in Fig. 2, the damage energy of intact and fissured clays can be obtained and listed in Table 7. Obviously, the damage energy of the clay can be little impacted by the fissure located in the middle of the upper edge and unrelated to the inclination of the middle fissure. While, compared with the damage energy of the intact clay, both fissures at right side of the upper edge or at the upper position of the right edge can reduce the damage energy of the fissured clay. In particular, the fissures at the right edge have the greatest impact.

Additionally, the maximum axial stresses listed in Table 7 are taken from the intersection site of the severely damage area of X-pattern. Under axial loads, except for T_{22} and T_{32}, other fissured clays have a trend, namely the damage energy is low, the maximum axial stress is high compared to the intact clay. For T_{22} and T_{32}, it may be the effect of obvious shear behavior causing low damage energy and low axial stress. Further future trials and simulations are needed to provide analysis and validation.

4. Conclusions

Based on test results under the uniaxial compression for the intact clay and nine fissured clay samples, the influence affected by the preset fissure on the failure form and local deformation of clays is studied. Meanwhile, the uniaxial compression simulation of the intact clay and nine fissured clay models is also discussed using the damage plasticity model. Compared with the compression results between test and the numerical method for clays, the following conclusions can be drawn.

- Among the three fissure positions, the fissure located on the right edge of clays has the greatest influence on the failure form and damage energy of clays, while for the three fissure angles, the 60-degree fissure has the greatest influence on the failure form. It is worth mentioning, the 60-degree fissure located on the right edge of the clay can reduce the compressive strength by 30%, compared with that of the intact clay.
- The damage plasticity model can basically simulate the compression behavior of clays containing a pre-existing fissure and reproduce the failure characteristics of clays. But there are still some differences, which can be further studied from two aspects: model quality and damage constitutive.
- Analyzing the evolution curves of the maximum principal stress-strain and shear stress-strain in the severely and slightly damaged areas of clays respectively, the preset fissure has obvious effect on the maximum principal stress of clays, but little effect on the shear stress.
- The numerical results also reveal that the maximum principal stress in the seriously damaged area of

the 60-degree fissured clay is lower than that in other clay samples.

Acknowledgments

Authors are wishing to acknowledge the financial support from the Science Research Fund of Nanjing Institute of Technology (No. CKJB201310).

References

Bayesteh, H. and Ghasempour, T. (2019), "Role of the location and size of soluble particles in the mechanical behavior of collapsible granular soil: A DEM simulation", *Comput. Part. Mech.*, **6**, 327-341. https://doi.org/10.1007/s40571-018-00216-x.

Borja, R.I. (2004), "Computational modeling of deformation bands in granular media. II. numerical simulations", *Comput. Meth. Appl. M.*, **193**(27-29), 2699-2718. https://doi.org/10.1016/j.cma.2003.09.018.

Castelli, M., Allodi, A. and Scavia, C. (2009), "A numerical method for the study of shear band propagation in soft rocks", *Int. J. Numer. Anal. Met.*, **33**, 1561-1587. https://doi.org/10.1002/nag.778.

Desrues, J., Chambon, R., Mokni, M., and Mazerolle, F. (1996), "Void ratio evolution inside shear bands in triaxial sand specimens studied by computed tomography", *Geotechnique,* **46**(3), 529-546. http://doi.org/10.1680/geot.1996.46.3.529.

Dong, Q.Q., Xiong, C.W, Ma, C.L. and Wei, H.J. (2019), "Experimental study on cracking behavior of intermittent double S-shaped fissures under uniaxial compression", *KSCE J. Civ. Eng.*, **23**(6), 2483-2494. https://doi.org/10.1007/s12205-019-1858-4.

Ebrahimian, B., Noorzad, A. and Alsaleh, M.I. (2018), "Modeling interface shear behavior of granular materials using micro-polar continuum approach", *Continuum Mech. Therm.*, **30**, 95-126. https://doi.org/10.1007/s00161-017-0588-4.

Huang, S.B., Yao, N., Ye, Y.C. and Cui, X.Z. (2019), "Strength and failure characteristics of rocklike material containing a large-opening crack under uniaxial compression: Experimental and numerical studies", *Int. J. Geomech.*, **19**(8), 04019098. https://doi.org.10.1061/(ASCE)GM.1943-5622.0001477.

Huang, Y.H., Yang, S.Q., Tian, W.L., Zeng, W. and Yu, L.Y. (2016), "An experimental study on fracture mechanical behavior of rock-like materials containing two unparallel fissures under uniaxial compression", *Acta Mech. Sin.*, **32**(3), 442-455. https://doi.org/10.1007/s10409-015-0489-3.

Huang, W. X., Huang, L. Y., Sheng, D.C. and Sloan, S. W. (2015), "DEM modelling of shear localization in a plane Couette shear test of granular materials", *Acta Geotech.*, **10**, 389-397. https://doi.org/10.1007/s11440-014-0348-6.

Jiang, M. J., Liu, J. and Shen, Z.F. (2018), "Investigating the shear band of methane hydrate-bearing sediments by FEM with an elasto-plastic constitute model", *B. Eng. Geol. Environ.*, **77**, 1015-1025. https://doi.org/10.1007/s10064-017-1109-1.

Kozicki, J. and Tejchman, J. (2018), "Relationship between vortex structures and shear localization in 3D granular specimens based on combined DEM and Helmholtz–Hodge decomposition", *Granul. Matter*, **20**, 48. https://doi.org/10.1007/s10035-018-0815-0.

Mühlhaus, H.B. and Alfantis, E.C. (1991), "A variational principle for gradient plasticity", *Int. J. Solids Struct.*, **28**(7), 845-857. https://doi.org/10.1016/0020-7683(91)90004-Y.

Schneider-Muntau, B., Chen, C. and Bathaeian, S.M.I. (2017), "Simulation of shear bands with Soft PARticle Code (SPARC) and FE", *Int. J. Geomath.*, **8**, 135-151. https://doi-org/10.1007/s13137-016-0091-2.

Vangla, P. and Latha, G.M. (2015), "Influence of particle size on the friction and interfacial shear strength of sands of similar morphology", *Int. J. Geosynth. Ground Eng.*, **1**, 6. https://doi-org/10.1007/s40891-014-0008-9.

Wanatowski, D. and Chu, J. (2006), "Stress-strain behavior of a granular fill measured by a new plane strain apparatus", *Geotech. Test. J.*, **29**(2), 1-9. https://doi.org/10.1520/GTJ12621.

Wang, B.J., Xiao, H.T. and Yue, Z.Q. (2012), "Interaction between two rectangular cracks in a transversely isotropic medium of semi-infinite extent", *Rock Soil Mech.*, **33**(8), 2527-2535. https://doi.org/10.16285/j.rsm.2012.08.001.

Wang, M., Cao, P., Wan, W., Zhao, Y. L., Liu, J. and Liu, J. S. (2017), "Crack growth analysis for rock-like materials with ordered multiple pre-cracks under biaxial compression", *J. Cent. South Univ.*, **24**, 866-874. https://doi.org/10.1007/s11771-017-3489-6.

Wang, X., Yuan, W., Yan, Y.T. and Zhang, X. (2020), "Scale effect of mechanical properties of jointed rock mass: A numerical study based on particle flow code", *Geomech. Eng.*, **21**(3), 259-268. https://doi.org/10.12989/gae.2020.21.3.259.

Watanabe, Y., Lenoir, N., Otani, J. and Nakai, T. (2012), "Displacement in sand under triaxial compression by tracking soil particles on X-ray CT data", *Soils Found.,* **52**(2), 312-320. https://doi.org/10.1016/j.sandf.2012.02.008.

Xu, J. and Li, Z.X. (2017), "Damage evolution and crack propagation in rocks with dual elliptic flaws in compression", *Acta Mech. Solida Sin.,* **30**, 573-582. https://doi.org/10.1016/j.camss.2017.11.001.

Yang, S.Q., Jing, H.W. and Xu, T. (2014), "Mechanical behavior and failure analysis of brittle sandstone specimen containing combined flaws under uniaxial compression", *J. Cent. South Univ.*, **21**, 2059-2073. https://doi.org/10.1007/s11771-014-2155-5.

CC